Int J Appl Earth Obs Geoinformation 85 (2020) 102007

Contents lists available at ScienceDirect

Int J Appl Earth Obs Geoinformation

journal homepage: www.elsevier.com/locate/jag

Discriminating treed and non-treed wetlands in boreal ecosystems using time series Sentinel-1 data

Zhan Li*, Hao Chen, Joanne C. White, Michael A. Wulder, Txomin Hermosilla

Canadian Forest Service (Pacific Forestry Centre), Natural Resources Canada, 506 West Burnside Road, Victoria, British Columbia, V8Z 1M5, Canada

ARTICLE INFO

Keywords:
Land cover
Monitoring
Synthetic aperture radar

ABSTRACT

Wetlands are recognized for their importance to a range of ecosystem goods and services; however, detailed information on wetland presence, type, extent, and persistence is challenging to attain over large areas and/or long time periods due to the spatial complexity and temporal dynamism of wetlands. In this study we explored the potential for within-year time series of C-band Synthetic Aperture Radar (SAR) observations from the free and open Sentinel-1 data archive to improve discrimination of treed and non-treed wetlands and non-wetlands in a boreal forest environment. Through a set of 3843 classification experiments for the year 2017, we tested the influence of three factors on classification accuracy: (i) input features (two backscatter coefficients in VV and VH polarization (σ_{VV} and σ_{VH}) and four quantitative measures derived from the Stokes vector); (ii) the temporal form of features (i.e. using all within-year observations versus generalized measures such as monthly/seasonal means or annualized statistics); and (iii) missing observations in Sentinel-1 time series due to varying observation availability across space. Among the tested features, we found the greatest utility in σ_{VV} and σ_{VH}. Directly using all within-year observations yielded higher accuracy than using generalized temporal forms. Moreover, the temporal form of the features had a greater impact on classification accuracy than the features themselves. The highest overall accuracy (0.860 ± 0.002) was achieved using σ_{VV} and σ_{VH} from all within-year observations. The majority of class confusion occurred between treed wetlands and non-wetlands. We found no significant reduction in the overall accuracy by simulated missing observations in time series when using all within-year observations. With the increasing availability of free and open data from the Sentinel-1 archive, new opportunities are emerging to readily integrate within-year time series into large-area land cover mapping, particularly if analysis-ready SAR data products further reduce preprocessing requirements for end users.

1. Introduction

Wetlands refer to areas that are inundated, whether naturally or artificially, permanently or temporarily, with static or flowing water that is fresh, brackish or salt, including marine water less than six meters in depth at low tide (Ramsar Convention Secretariat, 2013). The exact definition of wetlands varies between jurisdictions, organizations or disciplines but in essence, wetlands are subject to permanent or periodic inundation or prolonged soil saturation (Tiner, 2016). As the nexus between unsaturated terrestrial upland and aquatic deep water in the landscape mosaic (National Wetlands Working Group, 1997), wetlands are among the most productive environments and are of critical importance to both biological diversity and human wellbeing (Millennium Ecosystem Assessment, 2005; Ramsar Convention Secretariat, 2013). Wetlands are now recognized for the provision of a broad range of ecosystem services; however, the extent and viability of wetlands are increasingly threatened by land use change, pollution, and agricultural drainage, among others (Millennium Ecosystem Assessment, 2005). In this context, the need for comprehensive wetland inventories as well as monitoring capacity to identify status and trends is compelling as it provides the basis for guiding appropriate assessment, monitoring and furthermore management of wetlands (Dahl and Watmough, 2007; Davidson and Finlayson, 2007).

Wetland inventories typically characterize wetland location and extent, and also wetland classes according to the characteristics, environmental influences, functions, and/or uses (Davidson and Finlayson, 2007; Finlayson and van der Valk, 1995; Tiner et al., 2015). Various wetland classification schemes have been created, driven by different information needs. For example, the Canadian National Wetland Working Group categorizes wetlands into five major wetland classes including swamps, bogs, fens, marshes, and shallow water/ponds (Environment and Climate Change Canada, 2016; National

* Corresponding author.
E-mail address: zhanli1986@gmail.com (Z. Li).

https://doi.org/10.1016/j.jag.2019.102007
Received 14 August 2019; Received in revised form 22 October 2019; Accepted 28 October 2019

Wetlands Working Group, 1997). These five class definitions can be further simplified as treed wetlands (swamps) and non-treed wetlands (Canada's National Forest Inventory, 2017; Wulder et al., 2008). Wetlands are often captured as an ecological feature within other inventories, as is often the case for forest inventories. Canada's National Forest Inventory (NFI) reports the total area of forest and other wooded land with 12 broad land cover classes (Canada's National Forest Inventory, 2017; Wulder et al., 2008). The capacity to distinguish between treed and non-treed wetlands is an important information need for Canada's NFI as the distinction between treed and non-treed wetland impacts the reporting of treed area. Furthermore, treed status of wetlands is also helpful information to studying and modelling biological diversity, biogeochemistry and hydrology of wetlands (Matthews and Fung, 1987; Thogmartin et al., 2004; Toner and Keddy, 1997).

Although the need to inventory and monitor wetlands is well established, the methods and data sources used vary according to the area of interest and the level of detail required (Fournier et al., 2007). Field-based monitoring of wetlands is highly informative, yet temporally and spatially constrained, logistically challenging, and costly to operationalize over large or remote areas (Dahl and Watmough, 2007; Gallant, 2015). Therefore, wetland inventory and monitoring frequently avail upon remote sensing data and techniques due to comparatively lower costs and extensive spatial coverage (Davidson and Finlayson, 2007; Klemas, 2013; Lang and McCarty, 2008; Tiner et al., 2015). However, wetlands are a challenging target for classification using remotely sensed data due to their inherent dynamism and natural range of variability (Gallant, 2015; Tiner et al., 2015). The depth of water and the duration of its presence vary considerably from wetland to wetland and from year to year or even from season to season (Mitsch and Gosselink, 2007), which necessitates remotely sensed data with a higher temporal resolution than typically required to map other less dynamic land cover types.

While a variety of remotely sensed data types have been explored to determine their utility and address the aforementioned challenges in mapping wetlands (Klemas, 2013; Lang and McCarty, 2008; Tiner et al., 2015), two primary types of remotely sensed data for wetland mapping are multispectral optical images (Adam et al., 2010) and synthetic aperture radar (SAR) images (White et al., 2015) onboard satellite platforms. As optical remote sensing relies on solar illumination, weather conditions such as clouds and haze will obscure or contaminate acquired data and thus reduce available observations of the Earth's surface. In contrast, SAR is an active remote sensing technique that emits electromagnetic energy at microwave wavelengths and measures backscattered energy returned by Earth's surface (Henderson and Lewis, 2008), enabling data acquisition regardless of solar illumination, clouds, or haze (Lang and McCarty, 2008) and thereby increasing the frequency of useable observations. The amount of backscatter energy is primarily affected by the wavelength, polarization, and incidence angle of the microwave energy in combination with several key characteristics of the Earth's surface including dielectric property, size/roughness, and structure (Lang and McCarty, 2008). As such, SAR data relate to information particularly on soil moisture, inundation and vegetation structure owing to the sensitivity of microwave energy to water and its ability to penetrate vegetative canopies to various degrees depending on its wavelength (Tiner et al., 2015). Due to SAR's ability to collect data independent of prevailing illumination and cloud conditions (Lang and McCarty, 2008), the temporal resolution of available observations of Earth surface from SAR can be relatively higher than from optical sensors, given the same revisit frequency and imaging parameters (e.g., swath width).

Previous studies have noted the benefits to wetland mapping by using multi-temporal observations from multispectral optical sensors (Lunetta and Balogh, 1999; Zhang et al., 2017), SAR sensors (Banks et al., 2019; Brisco et al., 2011; Mahdavi et al., 2017; Martinez and Le Toan, 2007), or a combination of both (Bourgeau-Chavez et al., 2016; Corcoran et al., 2013; Töyrä et al., 2001). Earlier studies utilizing remotely sensed time series data over wetlands were often limited to relatively smaller spatial extents due to lack of data and burdensome data preprocessing needs, including co-registration, cross calibration, and quality screening. The recent advances in wetland mapping and change detection through time series observations at much larger scales (national, continental or global) (Pekel et al., 2016; Wulder et al., 2018; Yamazaki et al., 2015) are made possible not only by the recent substantial increases in the availability of multiple sources of medium-resolution satellite data over time but also by access to Analysis Ready Data (ARD) (Comber and Wulder, 2019). Landsat time series (LTS) data have been used and found valuable in the land cover mapping of Canada's vast forested ecosystems (Hermosilla et al., 2018, 2016). As a common land cover category in this ecosystem, the extent, distribution, and changing trends of wetlands over Canada's forested ecosystems have been specifically mapped using this harmonized time series of land cover maps (Wulder et al., 2018). On the other hand, limited access to SAR data and heretofore a lack of analysis-ready data products precluded the systematic use of time series of SAR data for wetland mapping at national, continental or global scales. However, the European Space Agency (ESA) now provides free and open access to the C-band SAR data from the Sentinel-1 satellites that observe the Earth in a systematic and operational fashion with short revisit time (Torres et al., 2012). This open access to the Sentinel-1 data archive with global coverage provides opportunities to leverage the temporal information from time series SAR data to map wetlands over larger spatial extents. Efforts towards Sentinel-1 ARD are on-going and will help to facilitate the use of SAR data in operational and large area applications (Truckenbrodt et al., 2019).

Whereas LTS data have demonstrated capacity for national wetland mapping and monitoring (Wulder et al., 2018), distinguishing between treed and non-treed wetlands over large areas is an important information need for forest ecosystem monitoring that remains challenging to address with LTS data alone. Hence, the objective of this study was to explore the potential of Sentinel-1 SAR within-year time series data to distinguish between treed and non-treed wetlands. Specifically, we seek to answer the following questions: (1) Which Sentinel-1 features provide the greatest utility for discriminating among the following three classes in boreal forest environments: treed wetlands, non-treed wetlands, and non-wetlands? (2) Which temporal form of these features provides the greatest accuracy (i.e. using all within-year observations or generalized measures such as monthly/seasonal means or annualized statistics)? (3) What impact do missing observations in within-year time series have on the accuracy with which these three classes can be discriminated? (4) What are the potential issues and opportunities associated with using within-year time series of Sentinel-1 data for spatially extending the methods applied herein to the national level?

2. Study area

The study area is a wetland-dominated region of the Hudson Plains ecozone in Canada (Fig.1). The Hudson Plains is strongly influenced by the cold and moisture laden Hudson-Bay-low and Polar-high air masses. With short cool summers and long cold winters, this lowland plain contains the largest extensive area of wetlands in the world that include extensive peatlands and shallow open water less than 2 m deep (Ecological Stratification Working Group, 1995). Forest are dominated by coniferous tree species, with spruce as the leading genus in 88% of all forest stands (Abraham and McKinnon, 2011). Dominant tree species include white spruce (*Picea glauca*) on dry sites, with willow (*Salix*), black spruce (*Picea mariana*), and tamarack (*Larix laricina*) more common on wetter sites. Forests in this ecozone are typically open and intermixed with wetlands, and canopy cover generally increases from north to south. Site productivity is low, with low wood volume per ha (42 m^3/ha) (Canadaös National Forest Inventory, 2010) and slow growth rates.

The area for this study is located in the eastern Hudson Plains and

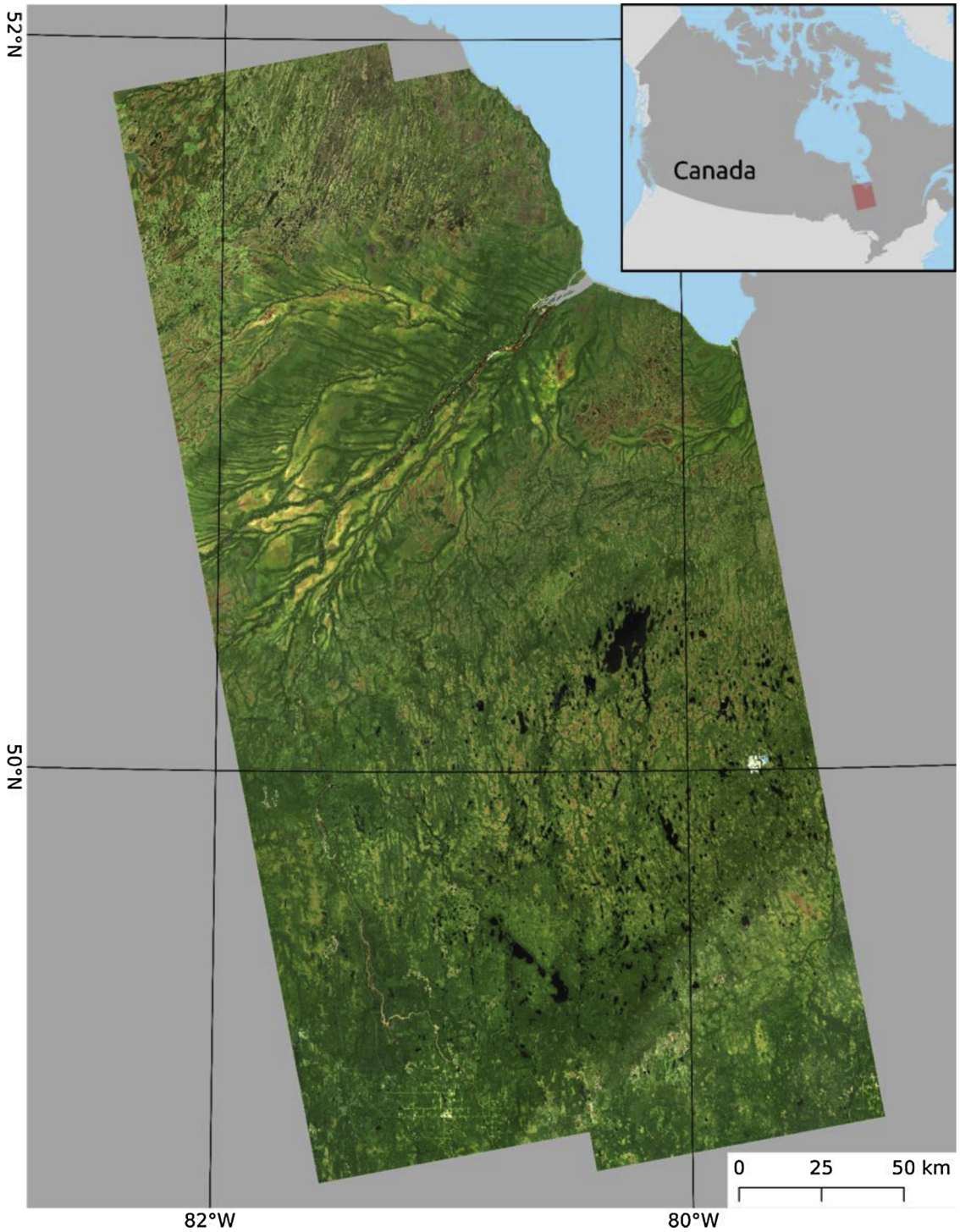

Fig. 1. Overview of the study area (the four Sentinel-1 sub-frames from two sub-swaths) in true-color image of annual gap-free best-available-pixel composites of Landsat surface reflectance for the year 2017.

corresponds to four sub-frames of two sub-swaths in the Sentinel-IW acquisition mode (Interferometric Wide mode, the main acquisition mode of Sentinel-1 over land (ESA, 2019a)). Each sub-frame covers 90 km (cross-track) ×170 km (along-track) and the total coverage of the four sub-frames is approximately 58,000 km^2. The landscape in this region has large areas of both treed and non-treed wetlands. A wetland area is considered treed if at least 10% of its area, by crown cover, consists of tree species of any size. Conversely, a wetland area is considered non-treed if less than 10% of its area, by crown cover, consists of trees species of any size (Canada's National Forest Inventory, 2017). Treed wetlands are located primarily in the north of this study area with non-treed found mostly in the south (see Fig. 2 and Section 3.2 for details). The occurrence of both treed and non-treed wetlands in this study area allows us to explore the discriminatory power of Sentinel-1 data from the operational IW acquisition mode for distinguishing between these two wetland classes.

3. Materials and methods

We examined the utility of Sentinel-1 features and their within-year

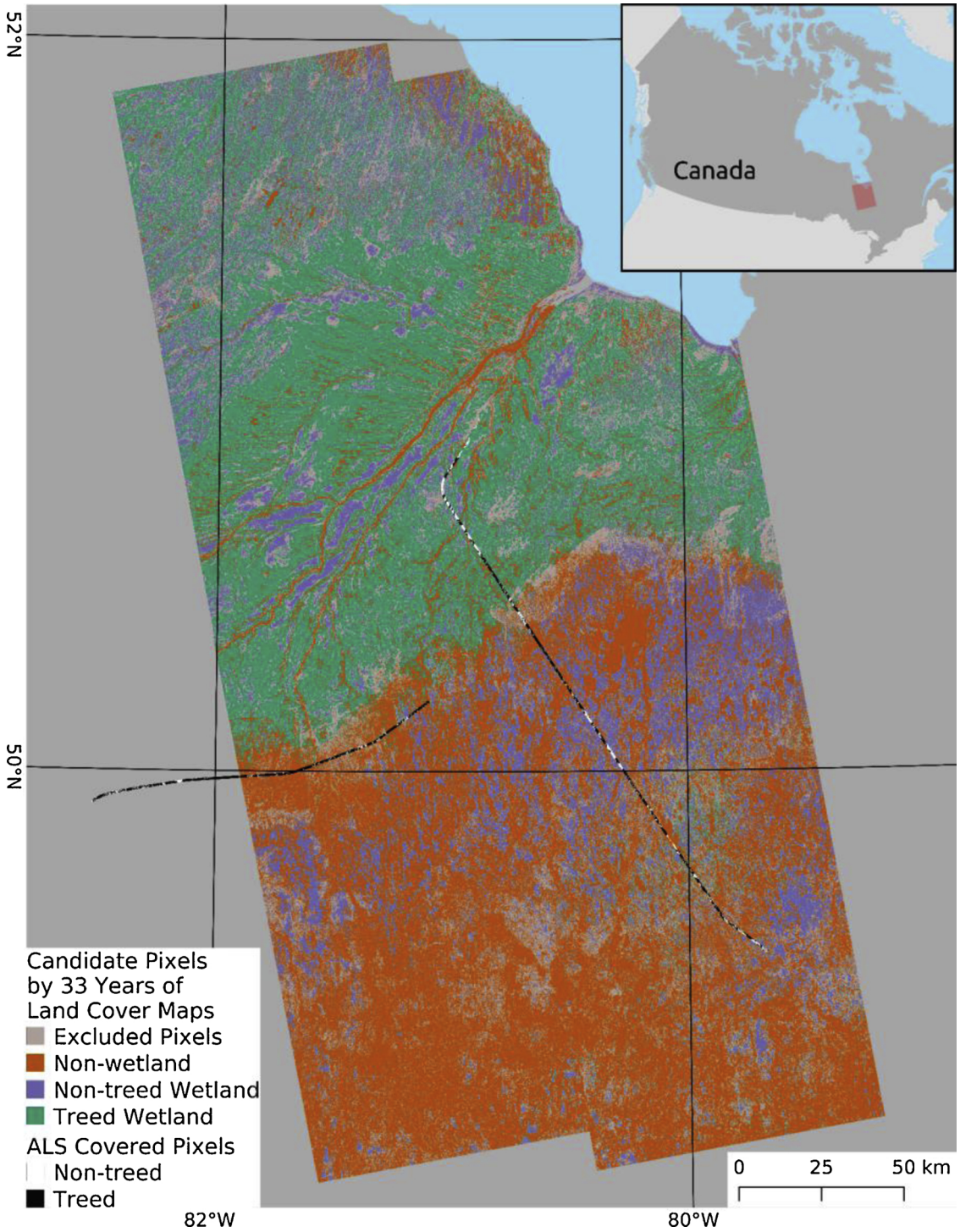

Fig. 2. Training and testing candidate pixels of wetland classes (treed and non-treed wetlands, and non-wetlands) that are delineated using the 33 annual land cover maps of Canada's forested ecosystems (Hermosilla et al., 2018; Wulder et al., 2018). Excluded pixels are those not persistently identified as treed wetlands, non-treed wetlands or non-wetlands by the 33 years of land cover maps. The airborne laser scanning (ALS) transects indicate treed status according canopy height and cover.

temporal information through a range of classification experiments using a Random Forest (RF) classifier (Breiman, 2001). We used two auxiliary datasets to facilitate the selection of pixels to train and test these classifiers, including 33 years of annual land cover maps and airborne-laser-scanning (ALS) based estimates of canopy structure. Lastly, we examined the impacts to classification by missing observations in Sentinel-1 time series through synthetic data with simulated missing observations.

3.1. Data

3.1.1. Sentinel-1 Synthetic Aperture Radar imagery time series

The Sentinel-1 satellites (A and B) carry C-band SAR instruments that routinely observe the Earth day-and-night under all weather conditions (Torres et al., 2012). The repeat cycle of observations for each Sentinel-1 satellite is 12 days and the two-satellite constellation could offer a 6-day repeat cycle if acquisitions were available from both satellites. This routine data acquisition, along with its free and open data

Table 1
List of Sentinel-1 features.

Feature	Description
σ_{VV}	Backscatter coefficient in VV polarization
σ_{VH}	Backscatter coefficient in VH polarization
S_1	First element of Stokes vector, approximately total power of the VV and VH channels
S_2	Second element of Stokes vector, approximately power difference between the VV and VH channels
m	Degree of polarization
μ_L	Linear polarization ratio

access, underpins the potential to extend our prototype investigation over the current study area to the entire Canada operationally. The main IW acquisition mode of the Sentinel-1 mission supports operations in dual polarization VV and VH (Torres et al., 2012), i.e. transmitting microwave energy in linear vertical (V) polarization and detecting returns in both linear vertical (V) and horizontal (H) polarization. The IW mode acquires observations from three sub-swaths (dubbed as IW1, IW2 and IW3). Observations from the three sub-swaths are acquired at different incidence angles that increase gradually from IW1, IW2 to IW3. The resultant SLC images therefore have slightly different spatial resolutions in both slant range (rg) and azimuth (az) dimensions. Owing to the limited coverage of one ancillary dataset (airborne lidar data) that we used to select training and testing pixels (see Section 3.1.2 for details), only sub-swaths IW1 and IW2 of the Sentinel-1 IW SLC products were used as our current study area. We obtained the Sentinel-1 IW Level-1 SLC products (IW acquisition mode, Single Look Complex) from the Copernicus Open Access Hub (European Union Copernicus, 2019). We chose to use the Level-1 SLC products because they contain both backscatter intensity and phase information, allowing the use of Stokes vector approaches to explore potential Stokes vector features that may help differentiate treed and non-treed wetland classes. In total for the year of 2017, Sentinel-1B satellite provided the IW SLC products on 23 dates representing all the seasons for all pixels over our study area; however, no data was available from Sentinel-1A.

3.1.2. Annual land cover maps and airborne-laser-scanning based estimates of canopy structure

We used two datasets to facilitate the selection of pixel samples to train and test wetland classifiers, including annual land cover maps of 33 years (1984 to 2016) and ALS based estimates of canopy structure. The annual land cover maps were generated using the Virtual Land Cover Engine (VLCE) from a time series of annual gap-free best-available-pixel composites of Landsat surface reflectance and auxiliary topographic data (Hermosilla et al., 2018). After generating preliminary annual land cover classifications using a RF classifier, the VLCE approach further reduced spurious land cover transitions per pixel through time via a Hidden Markov Model (Abercrombie and Friedl, 2016) that utilized forest change information and expert-based class transition probabilities. This process produced the change-informed and temporally integrated annual land cover maps that we used in this study. The 25-m raster products of canopy height and cover estimates were generated from ALS acquisitions in the summer of 2010. The ALS data had a pulse density of approximately 3 points/m^2 from which point cloud metrics were generated at a grid cell resolution of 25 m, as detailed in Wulder et al. (2012). The 99th percentile of heights of first returns above 2 m was used to represent canopy height, and the percentage of returns above 2 m was used to estimate canopy cover for each grid cell. The ALS point cloud metrics were resampled into the 30-m grid of the annual land cover maps using bilinear interpolation.

3.2. Selection of training and testing pixels

The annual VLCE land cover maps and the ALS-based canopy structure estimates provided *a priori* information on the location and extent of wetlands and their treed status and were used as strata to select a set of training and testing pixels for RF classifier training and testing. We selected treed wetland candidate pixels as those that were identified as treed wetland by all the 33 years of land cover maps and also as treed by the ALS data according to the FAO's definition of forests (treed areas are those with canopy height greater than 5 m and canopy cover greater than 10% (FAO, 2012)). Similarly, we selected non-treed wetland candidate pixels for training and testing as those identified as non-treed wetlands by all the 33 years of land cover maps and also as non-treed by the ALS data. Non-wetland candidate pixels for training and testing were those pixels that were not identified as wetlands by any of the 33 years of annual land cover maps, independently of being determined as treed or non-treed by the ALS data. The selection excluded pixels that were not persistently identified as treed wetlands, non-treed wetlands, or non-wetlands within the 33 years of VLCE land cover maps. This selection practice accumulated evidence about land cover over time and also restricted training and testing samples to areas that have not changed, according to the Landsat time series. Hence it minimized the impact of applying the ALS data acquired in 2010 to the Sentinel-1 data acquired in 2017. In total for training and testing, 0.04% of the study area was identified as candidate areas for treed wetlands, 0.03% for non-treed wetlands, and 0.14% for non-wetlands. We randomly selected two thirds of all candidate pixels in each class to train the RF classifier and the remaining one third as testing data to evaluate the accuracy of wetland classifications and hence the utility of Sentinel-1 features and their temporal information.

3.3. Preprocessing of Sentinel-1 SAR data

We used the ESA Sentinel Toolboxes (SNAP) (ESA, 2019b) and processed each Sentinel-1 SLC product into six Sentinel-1 features (Table 1) including, VV and VH backscatter coefficients (σ_{VV} and σ_{VH}), the first two elements of the Stokes vector (S_1 and S_2), the Degree of Polarization (m), and the Linear Polarization Ratio (μ_L) (Raney, 2006). The processing to generate the radar backscatter coefficients (σ_{VV} and σ_{VH}) included the following seven steps: (1) "TOPSAR-Split" (split sub-swath IW1 and IW2); (2) "Apply-Orbit-File" (obtain precise orbital information); (3) "Calibration" (calculate backscatter coefficients σ_{VV} and σ_{VH}); (4) "TOPSAR-Deburst" (remove demarcation zone between two bursts); (5) "Multilook" (generate one square pixel from 4 rg × 1 az looks); (6) "Speckle-Filter" (reduce speckle noise using Lee Sigma Filter (Lee et al., 2009)) and (7) Terrain Correction using SRTM 1 arc-second Digital Elevation Model (~30 m) (NASA JPL, 2019) before resampling the raster data into the projection of UTM-17S zone at 30-m pixel resolution using bilinear interpolation.

The processing to generate Stokes vector features from the SLC data firstly followed the aforementioned steps (1) to (5) for backscatter coefficients, except that step (3) of "Calibration" outputted complex numbers instead of backscatter coefficients to keep the phase information. Subsequently three additional steps were applied: (6) form a 2-pixel × 2-pixel average wave covariance matrix of the backscattered field (Cloude et al., 2012) before applying a polarimetric speckle filter, the Refined Lee Filter (Yommy et al., 2015), to the matrix; (7) per pixel, calculate a four-element real Stokes vector $[S_1 \;\; S_2 \;\; S_3 \;\; S_4]^T$ (we adopted S_1 and S_2 in this study) and two Stokes-vector-based parameters, Degree of Polarization (m) and Linear Polarization Ratio (μ_L) (Raney, 2006); (8) terrain correct the two elements of the Stokes vector and the derived parameters using the same procedures as above for backscatter coefficients.

All the derived Sentinel-1 features were stacked and then aligned with the 30-m raster grid of the annual land cover maps in the projection of UTM-17S zone. We assured the fidelity of georegistration among the time series images of Sentinel-1 and also between them and the Landsat-based land cover maps after visually examining the alignment of artificial targets, such as roads and airport.

Although SAR signals from the two sub-swaths are potentially influenced by their different incidence angles (Tsyganskaya et al., 2018), we did not observe clear artifacts caused by incidence angles in the images of the six Sentinel-1 features between the two sub-swaths used in our analysis, likely because the differences in incidence angles between the two adjacent sub-swaths are relatively small (the nominal incidence angle for the Sentinel-1 IW products is 32.9° for IW1 and 38.3° for IW2 (ESA, 2019c)). Meanwhile, considering the limited training and testing pixels available over the two sub-swaths, we used all the training pixels across the two sub-swaths (IW1 and IW2) together to train one RF classifier and apply the trained classifier to both sub-swaths in each experiment of RF classification as described in the next section.

3.4. Experimental design of wetland classification using Random Forests classifier

For the classification of wetlands using the derived Sentinel-1 SAR data, we used the RF classifier, which draws random subsets of training samples and predictor variables to produce multiple decision trees to form an ensemble classification (Breiman, 2001). The RF classifier is a robust, non-parametric classifier that has been applied extensively for land cover mapping applications (Belgiu and Drăgu, 2016). In this study, we used an implementation of RF classifier in the Python Scikit-learn package (Pedregosa et al., 2011).

To examine the utility of the six Sentinel-1 features (σ_{VV}, σ_{VH}, S_1, S_2, m, μ_L) (Table 1) and their temporal information, we designed multiple experiments in which RF classifiers used different predictor sets comprising different combinations of the Sentinel-1 features and different forms of their temporal information. We had 63 combinations of Sentinel-1 features, that is, $\binom{6}{1}+\binom{6}{2}+\binom{6}{3}+\binom{6}{4}+\binom{6}{5}+\binom{6}{6}$, corresponding to the use of one to six selected features from the total six features (Table 2). For the forms of the temporal information in Sentinel-1 features, we tested the following five types of temporal metrics: (1) one observation from a random observation cycle in each of selected seasons, (2) observations from available repeat observation cycles in each of selected seasons, (3) monthly means of available observations in each of selected seasons, (4) seasonal means of available observations in each of selected seasons, and (5) annualized statistics of available observations in the entire year (similar to those used in Hansen et al. (2016;, 2013)) including, minimum, maximum, and selected percentiles (10, 25, 50, 75, 90 percentiles) of within-year observations, and mean values of observations between selected percentiles (minimum-10%, 10–25%, 25–50%, 50–75%, 75–90%, 90%-maximum, minimum-maximum, 10–90%, and 25–75%). The definition of seasons was calendar based for simplicity and applicability over large areas, i.e., March-April-May (MAM) as spring, June-July-August (JJA) as summer, September-October-November (SON) as autumn, and December-January-February (DJF) as winter. There are 15 combinations of the four seasons, that is, $\binom{4}{1}+\binom{4}{2}+\binom{4}{3}+\binom{4}{4}$. Each of the first four types of temporal metrics has 15 temporal forms from choosing different combinations of the four seasons while the last type of temporal metrics, annualized statistics, has one temporal form from using all the four seasons. In total, we considered Sentinel-1 features in 61 different temporal forms as candidate predictors in the classification experiments (Table 2).

With the feature combinations (63) and temporal forms (61) for each combination, we created $63 \times 61 = 3843$ different sets of predictors to test in the classification experiments. In each experiment with a given set of predictors, that is, selected Sentinel-1 features of one combination in one temporal form, we optimized the number of decision trees in a RF classifier (*ntree*) and the number of predictor variables to be selected to build each tree (*mtry*) (Belgiu and Drăgu, 2016). We then selected the *ntree* and *mtry* values that yielded the best 3-fold cross-validation result over the training pixels to build the final RF classifier in each experiment. Meanwhile, to balance training pixel counts among classes, we used the same number of training pixels per class as the smallest training pixel counts of the three classes, that is, 15,740 pixels in our case. We then randomly selected 15,740 pixels without replacement from all available training pixels in each of the other two classes to use in the RF training. For each of the 3843 experiments, we applied the trained RF classifier to the withheld testing pixels and estimated the overall, user's and producer's accuracy to evaluate the performance of each RF classifier and hence each predictor set (selected features in a selected temporal form).

3.5. Analysis and comparison of outcomes of classification experiments

To examine the utility of Sentinel-1 features in wetland classifications, we grouped and compared the accuracy measures of RF classification results from all the experiments by the combinations of Sentinel-1 features. Each feature combination includes all of the examined temporal forms for each feature. For each accuracy measure (overall accuracy, and user's and producer's accuracies per class), we sorted the feature combinations according to the highest achieved accuracy given each feature combination, where we checked which Sentinel-1 features appeared more often in classifications of higher accuracies. To better demonstrate the importance of Sentinel-1 features to our classification, we identified the pairs of classifications that only differed by whether a given Sentinel-1 feature was included in or excluded from an experiment. We calculated the accuracy difference per each pair as an indicator of Sentinel-1 feature importance.

Similarly, to examine the contribution of observations in different temporal forms and different seasons to wetland classifications, we grouped and compared the accuracy measures of RF classification results from all the experiments by temporal forms. For each temporal form, we grouped all the examined feature combinations. For each accuracy quantity (overall accuracy, and user's and producer's accuracies per class), we sorted the temporal forms according to the highest achieved accuracy under each temporal form, where we checked which temporal forms appeared more often in classifications of

Table 2
List of feature combinations and temporal forms. One set of predictors comes from choosing one combination of Sentinel-1 features and one temporal form.

Feature Combinations	Temporal forms per each feature combination
• Using 1 feature: 6 combinations • Using 2 features: 15 combinations • Using 3 features: 20 combinations • Using 4 features: 15 combinations • Using 5 features: 6 combinations • Using 6 features: 1 combination	• Using one random observation per each of selected seasons: 15 forms • Using all available observations per each of selected seasons: 15 forms • Using monthly means of observations per each of selected seasons: 15 forms • Using seasonal means of observations per each of selected seasons: 15 forms • Using annualized statistics below: 1 form ○ Minimum & Maximum ○ 10, 25, 50, 75, 90 percentiles ○ Mean of observations between (minimum-10%, 10-25%, 25-50%, 50-75%, 75-90%, 90%-maximum, minimum-maximum, 10-90%, and 25-75%).

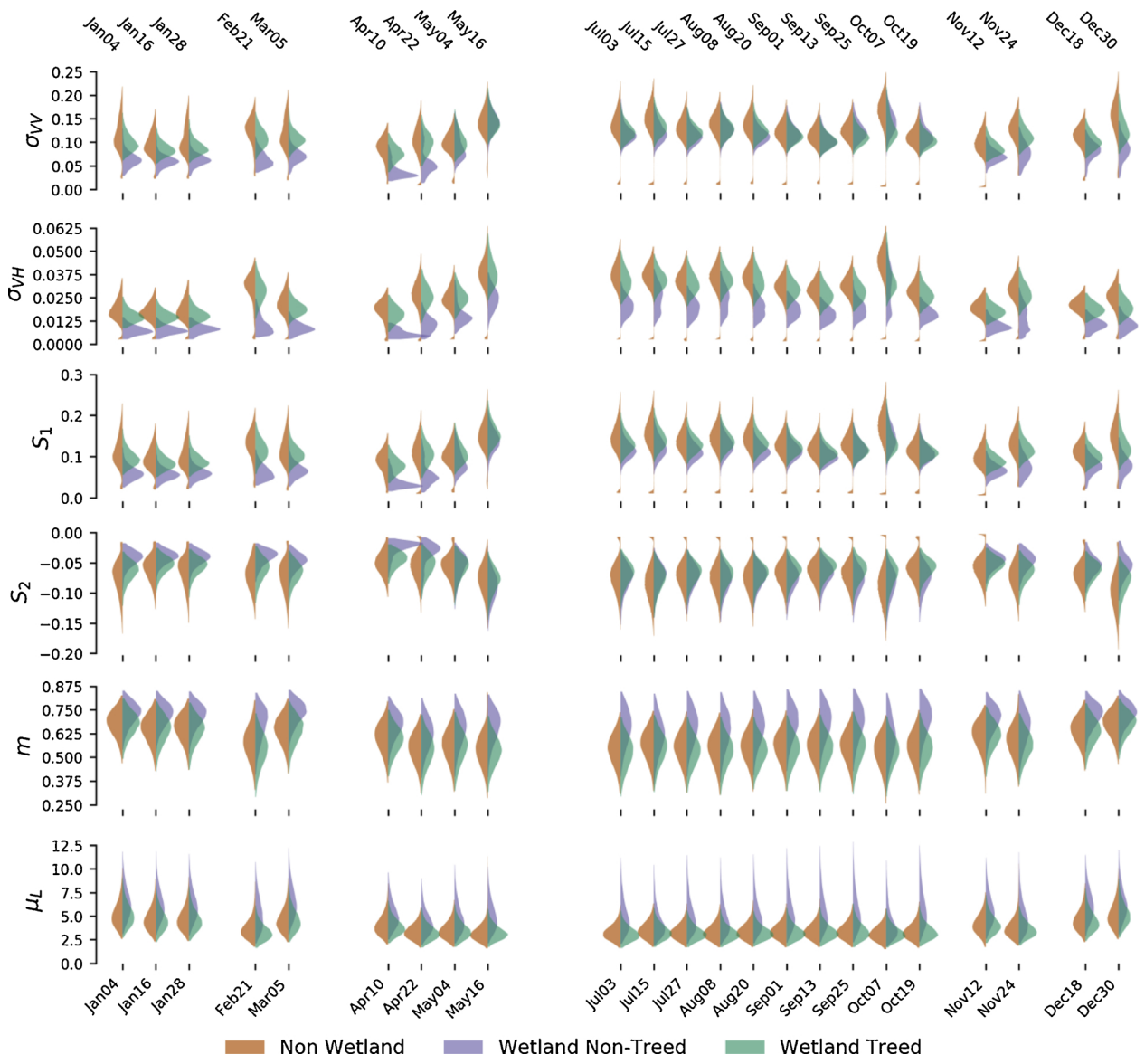

Fig. 3. Distribution of values of six Sentinel-1 features per non wetland, non-treed wetland and treed wetland pixels.

higher accuracies. To better demonstrate the importance of seasons to the wetland classification, we found the pairs of classifications that only differ by whether a given season was included in or excluded from a classification experiment. We calculated the accuracy difference per each pair as an indicator of importance of seasons.

3.6. Examination of impacts to classifications by missing observations in Sentinel-1B time series

Every pixel in the study area has observations from the same 12-day repeat observation cycles of the Sentinel-1B satellite. However, if we subsequently attempt to apply the optimal classification model identified herein to a much larger area (e.g. at the ecozone level or nationally), multiple Sentinel-1 swaths will be required and not all pixels will have available observations from the same repeat cycles. In other words, temporal frequency of available observations may be irregular in different pixels with some areas covered by more observations and others by fewer. Although it matters less for the temporal forms of using monthly means, seasonal means and annualized statistics to have observations from the same repeat cycles, missing observations in Sentinel-1 times series alter values of temporal metrics in these temporal forms and hence may still impact the classification performances. Such missing observations in a within-year time series are likely to be common when classifying large areas that have varying observation availability across space. Therefore, to examine the impact of missing observations in Sentinel-1 time series on classification outcomes, we created a synthetic dataset by randomly removing observations of a few repeat cycles per pixel in both training and testing data. The random selection of observations to be removed followed a Bernoulli distribution with the probability of being selected as 0.24. This random simulation of missing observations means the number of missing observations per pixel was random and not necessarily the same in different pixels across space. Rather, the expectation of numbers of missing observations over all pixels was set as 0.24 fraction of 23 observations (i.e., ~6 observations). This missing probability of 0.24 was determined as the ratio between 23—the current actual number of available observations from the Copernicus Open Access Hub—and 30.4, the expected number of total observations given the 12-day repeat cycle of one Sentinel-1 satellite (Torres et al., 2012). Then we repeated the classification experiments using the training and testing data with simulated missing observations. When predictor values of some pixels in an experiment were unavailable due to missing observations in the

synthetic dataset, we filled predictor values of these pixels before including them in RF classifiers. As the findings from this prototype study were intended to inform wetland mapping over large areas such as the entire Canada, some simple and fast algorithms of data filling were preferred over sophisticated but slower ones. Therefore, for the temporal forms of using individual observations, monthly means, and seasonal means, we filled missing values in a set of predictors per pixel by using a simple linear interpolation along time axis. For the temporal form of using annualized statistics, we filled missing values in the sets of predictors by simply using the mean of each statistical predictor. We ran the simulation of missing observations for 50 times to create 50 synthetic datasets from which we obtained 50 classifications and then reported the mean accuracy of these classifications. To quantify the impact of missing observations in the Sentinel-1 time series for this study, we checked the differences of classification accuracies for the selected top-performing sets of predictors between using the original dataset and using the synthetic dataset with simulated missing observations.

4. Results

In the following, we first present the distributions of Sentinel-1 feature values on each acquisition date throughout the year for the classes of our interest, treed and non-treed wetlands and non-wetlands. We then grouped and compared the accuracy measures of RF classification results from all the experiments by feature combinations to illustrate the importance of each Sentinel-1 feature to classification outcomes. Then, we grouped and compared the accuracy measures of RF classification results from all the experiments by their temporal forms to illustrate which temporal form yielded the best classification outcome. Lastly, we present and analyze the impact of simulated missing observations from the Sentinel-1 time series on classification outcomes before presenting a classification and its accuracy assessment from using the best-performing Sentinel-1 feature combination and temporal form.

4.1. Distribution of Sentinel-1 feature values throughout the year

Fig. 3 presents the value distributions of the six Sentinel-1 features (σ_{VV}, σ_{VH}, S_1, S_2, m, μ_L) of treed wetland, non-treed wetland, and non-wetland pixels per acquisition date throughout the year. The distributions were smoothed by kernel density estimation. These distributions illustrated the potential capacity of each of these Sentinel-1 features to discriminate our target classes. In the feature σ_{VH}, we observed the strongest separation between treed and non-treed wetlands compared to the other features throughout the year in all the seasons. The σ_{VV} also separated treed and non-treed wetlands well but only during the time from January to April and November to December, the wetter and colder seasons of the year in this study area. Among the four Sentinel-1 features based on Stokes vectors, the S_1 (the first element of Stokes vector), that is approximately the total power of the VV and VH channels (Raney, 2006), exhibited sufficient separation between the wetland classes during the wetter seasons, similar to the σ_{VV}. The m (degree of polarization) also offered some separation between the wetland classes throughout the year. The S_2 (the second element of Stokes vector, the power difference between the VV and VH channels) and the μ_L (linear polarization ratio) seemed insufficient information to separate treed- and non-treed wetlands. In general, the separation between wetlands and non-wetlands was weak and the distributions of all the six Sentinel-1 features over non-wetlands and treed wetlands overlapped each other throughout the year.

4.2. Comparison of classifications using different combinations of Sentinel-1 features

Fig. 4 displays accuracy measures of all the classification experiments using different feature combinations sorted by the highest achieved accuracy given a feature combination for each accuracy measure (overall accuracy, and user's and producer's accuracies per class). Each feature combination includes all of the examined temporal forms for each feature, and a wide distribution in accuracies was observed for each feature combination (Fig. 4). Across all feature combinations, the inclusion of σ_{VH} and σ_{VV} were consistently associated with the higher accuracies indicating the utility of these features in discriminating among our target classes. The accuracy measures do not change markedly among the different feature combinations on the left of x-axis in Fig. 4, but do decrease markedly once both σ_{VH} and σ_{VV} are excluded from the feature combinations.

Fig. 5 displays the distribution of changes in accuracy due to the inclusion of a particular Sentinel-1 feature in the classification along with several statistics of the accuracy changes (the mean, median, and percentiles). The distributions of changes in all the accuracy quantities are almost always positive, with long tails of large positive values (indicating that accuracy is higher when the feature is included), suggesting that all the Sentinel-1 features carry some information for discriminating our target classes. However, the tails of positive changes have much higher density of values for the σ_{VH}, σ_{VV}, S_1 and S_2 than for the m and μ_L, suggesting different levels of the usefulness among the Sentinel-1 features. The means and medians of accuracy changes indicate the feature importance is highest for the σ_{VH} and σ_{VV}, followed by the S_1 while including S_2, m, or μ_L does not make significant improvements in classification accuracies.

4.3. Comparison of classifications using different forms of temporal information

Fig. 6 displays the accuracy measures of all the classification experiments using different temporal forms sorted by the highest achieved accuracy under a given temporal form for each accuracy quantity (overall accuracy, and user's and producer's accuracies per class). Notably the distributions of accuracies associated with each temporal form (Fig. 6) are much narrower than those associated with each feature combination (Fig. 4). Among the four seasons, there is no single season that consistently provides higher accuracies, supporting the usefulness of temporal information over an entire year for Sentinel-1 features. Indeed, we observed higher accuracies for temporal forms that incorporated observations from all four seasons, with decreasing accuracy for temporal forms that included fewer seasons, especially for overall accuracy, producer's accuracy of non-wetlands, and user's accuracy of treed wetlands (Fig. 6).

Temporal forms that used all available within-year observations resulted in higher accuracies than the other temporal forms (i.e. one random observation per season, monthly means, seasonal means or annualized statistics). Although in some instances the highest accuracy of using a single random observation per season is acceptable, the distribution of accuracy values is much wider than when other temporal forms are used in the classification, suggesting that classification performance is unreliable when using only one observation per season. Likewise, monthly or seasonal averages result in lower accuracies than if all available observations are used.

Fig. 7 displays the distribution of accuracy changes due to including a season in the classifications along with several statistics of the accuracy changes (the mean, median, and percentiles). The distributions of changes in all the accuracy quantities are almost all on the positive side of y-axis with long tails of large positive values (accuracy increase when including a season), suggesting all the seasons within a year carry some information for wetland classification. The wetter seasons of our study area, spring (MAM) and winter (DJF) demonstrate slightly higher importance than the drier seasons, summer (JJA) and autumn (SON). The JJA has the lowest importance, however, probably due to observation missing in the entire month of June (Fig. 3).

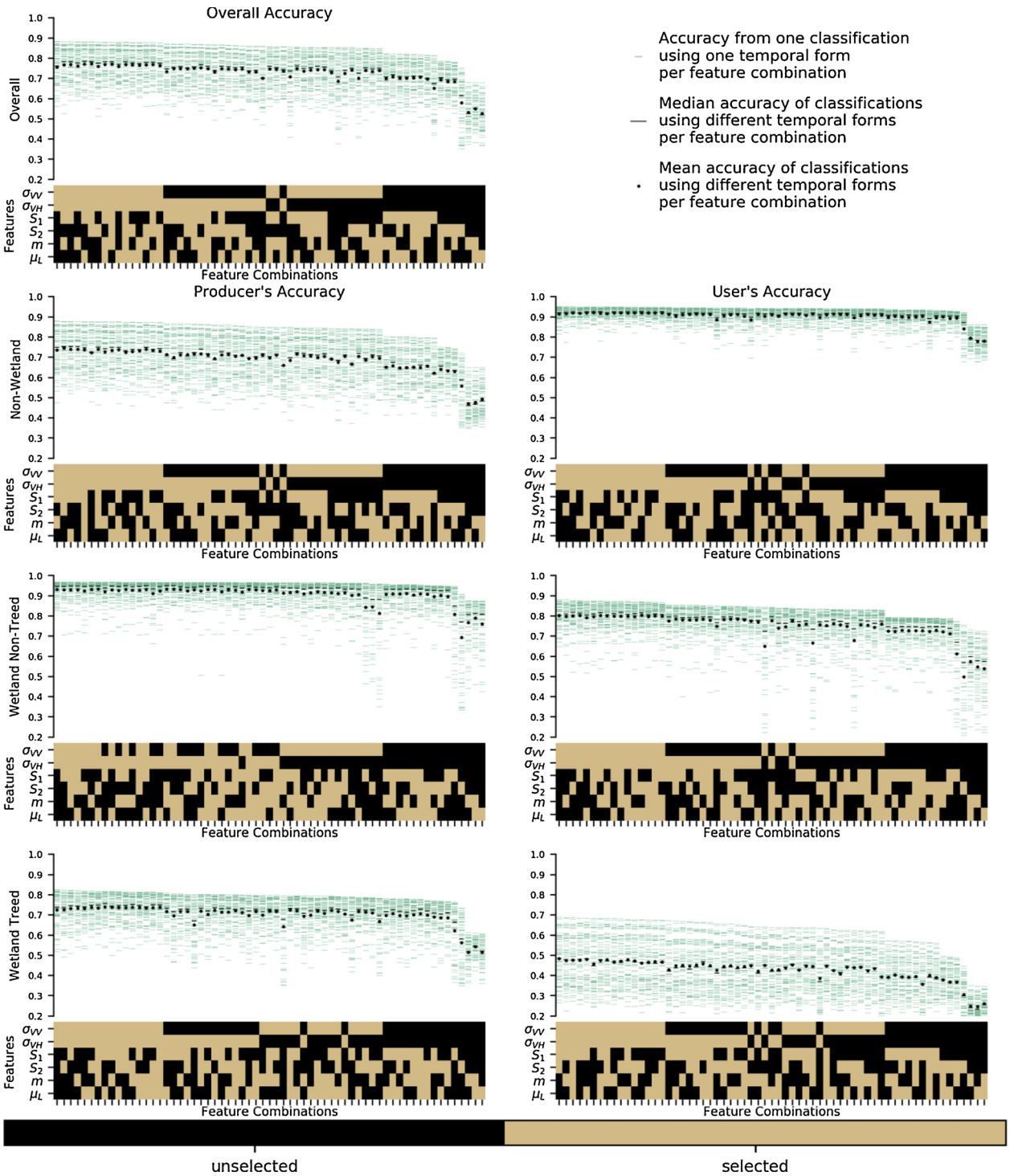

Fig. 4. Classification accuracies versus different combinations of the six Sentinel-1 features. The combinations in each panel are sorted according to the highest accuracy among using different temporal forms per feature combination.

4.4. Changes in classification accuracies due to missing observations in Sentinel-1 time series

We investigated the impact to wetland classifications due to missing observations in Sentinel-1 time series for all the Sentinel-1 feature combinations using the four temporal forms that use all available observations of all the seasons, monthly means of all the seasons, seasonal means of all the seasons and the annualized statistics of observations in the entire year (Fig. 8). Surprisingly, not all the accuracy quantities decrease when missing observations occur in the within-year time series. The overall accuracies for the four temporal forms often resulted in no change in accuracy or a slight increase. The producer's accuracy of non-wetlands and the user's accuracy of treed and non-treed wetlands increases when using a synthetic dataset with simulated missing observations in the classification. In contrast, missing observations cause expected decreases in the user's accuracy of non-wetlands and the producer's accuracy of non-treed wetlands, and particularly large decreases in the producer's accuracy of treed wetlands. Across the four examined temporal forms, the patterns of changes in accuracy due to missing observations are similar for most accuracy quantities. For the

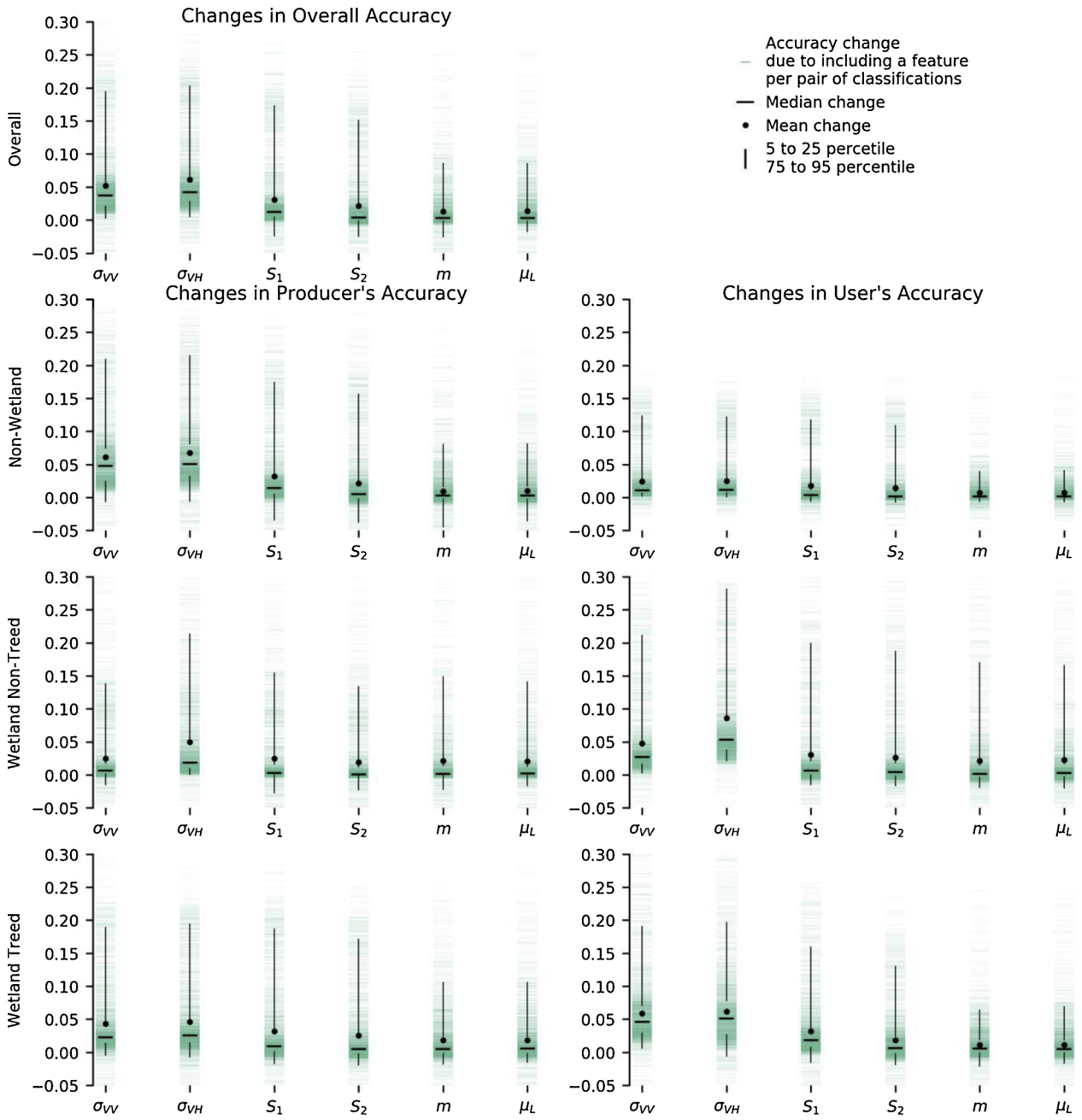

Fig. 5. Changes in classification accuracies between using and not using each Sentinel-1 feature.

producer's accuracy of treed wetlands and the user's accuracy of non-wetlands, using all available observations or monthly means resulted in smaller accuracy decreases than using seasonal means or annualized statistics. There was not much difference in the accuracy changes due to missing observations across the different combinations of Sentinel-1 features.

4.5. Classification results using best-performing feature combination and temporal form

According to the aforementioned comparison of Sentinel-1 feature combinations and temporal forms, we identified the best-performing classification by directly using σ_{VH} and σ_{VV} from all available observations over the entire year of 2017 in this study. The overall accuracy of this classification (Fig. 9) is approximately 0.860 ± 0.002 (Table 3) based on the assessments using test pixels and the class proportions in the classification map.

5. Discussion

Acknowledging the challenges to systematically produce large-area classifications of wetlands and different wetland classes, a target that is spatially complex and temporally variant, we examined the utility of free and open Sentinel-1 IW SLC products with operational global coverage and their within-year temporal information to discriminate treed and non-treed wetlands and non-wetlands. To this end, we analyzed the relative importance of six Sentinel-1 features and their temporal forms for wetland classifications as well as the impact of missing observations on classification outcomes.

Among the six Sentinel-1 features we examined, we identified σ_{VH} and σ_{VV} as the two most important Sentinel-1 features for differentiating between treed and non-treed wetlands. This result from the

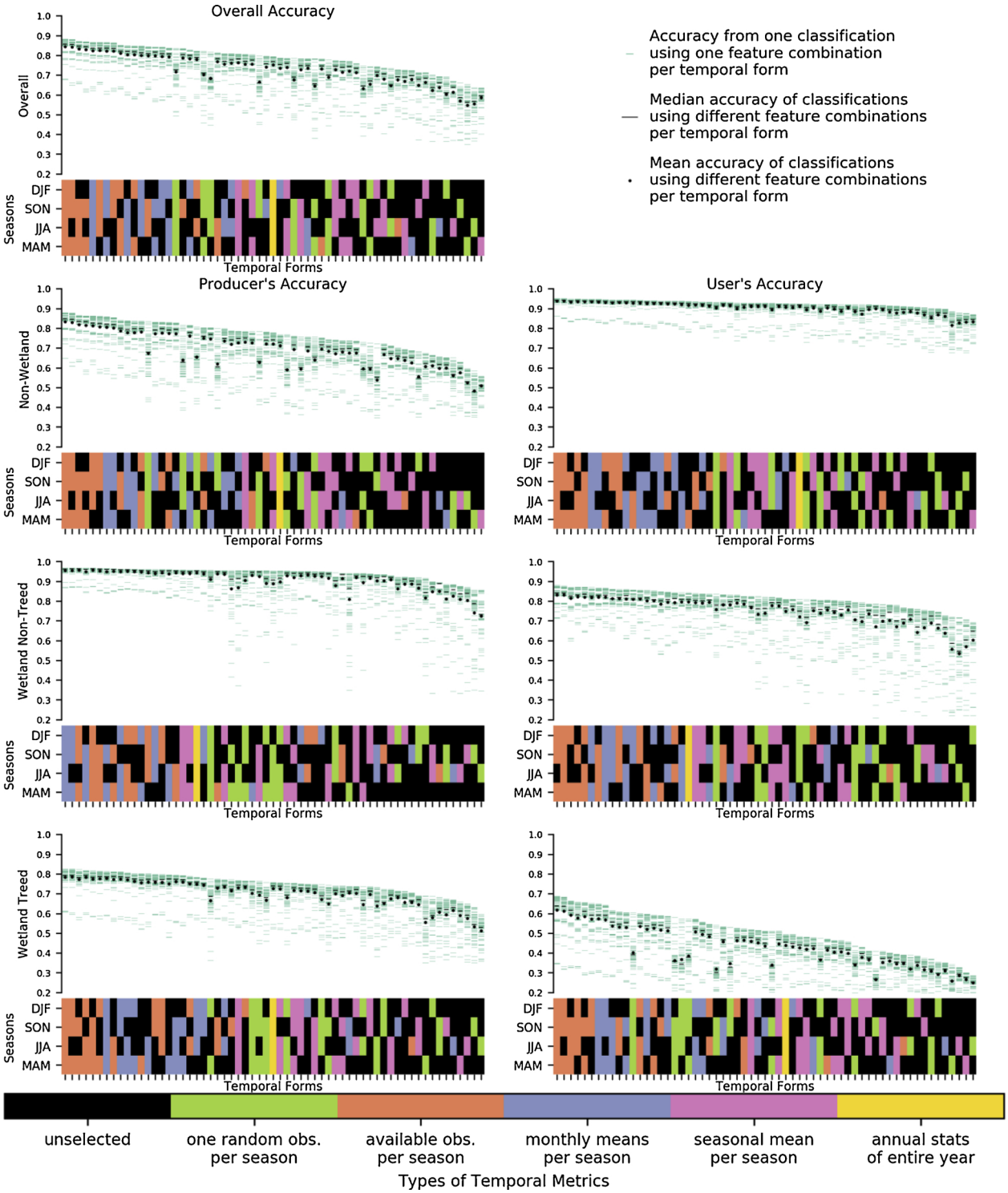

Fig. 6. Classification accuracies versus different temporal forms, i.e. different temporal metrics in different combinations of seasons. The temporal forms in each panel are sorted according to the highest accuracy among using different feature combinations per temporal form.

comprehensive set of 3843 classification experiments is in line with the separability of our target classes that we observed from examining the distributions of the Sentinel-1 feature values (Fig. 3). The benefits of combining both co-polarized (such as the VV) and cross-polarized (such as the VH) backscatter coefficients has been reported in classifying wetlands before for C-band SAR data (Amani et al., 2019; Brisco et al., 2013, 2011; Zhao et al., 2014). The ability of σ_{VH} to separate treed and non-treed wetlands is related to the sensitivity of σ_{VH} to volume scattering that depends largely on the vegetative canopy structures and hence differs between treed and non-treed vegetation (Freeman and Durden, 1998; Tsyganskaya et al., 2018). This difference in canopy structures exists throughout the year between treed and non-treed wetlands in our study area and thereby so does σ_{VH} (Fig. 3). In contrast, the difference in σ_{VV} between treed and non-treed wetlands only exists during wetter seasons of the year likely because the σ_{VV} is sensitive to the presence of surface water, wet snow, or ice surface underneath vegetative canopies (Brisco et al., 2011; Tsyganskaya et al., 2018). The relatively large increases in classification accuracies due to including

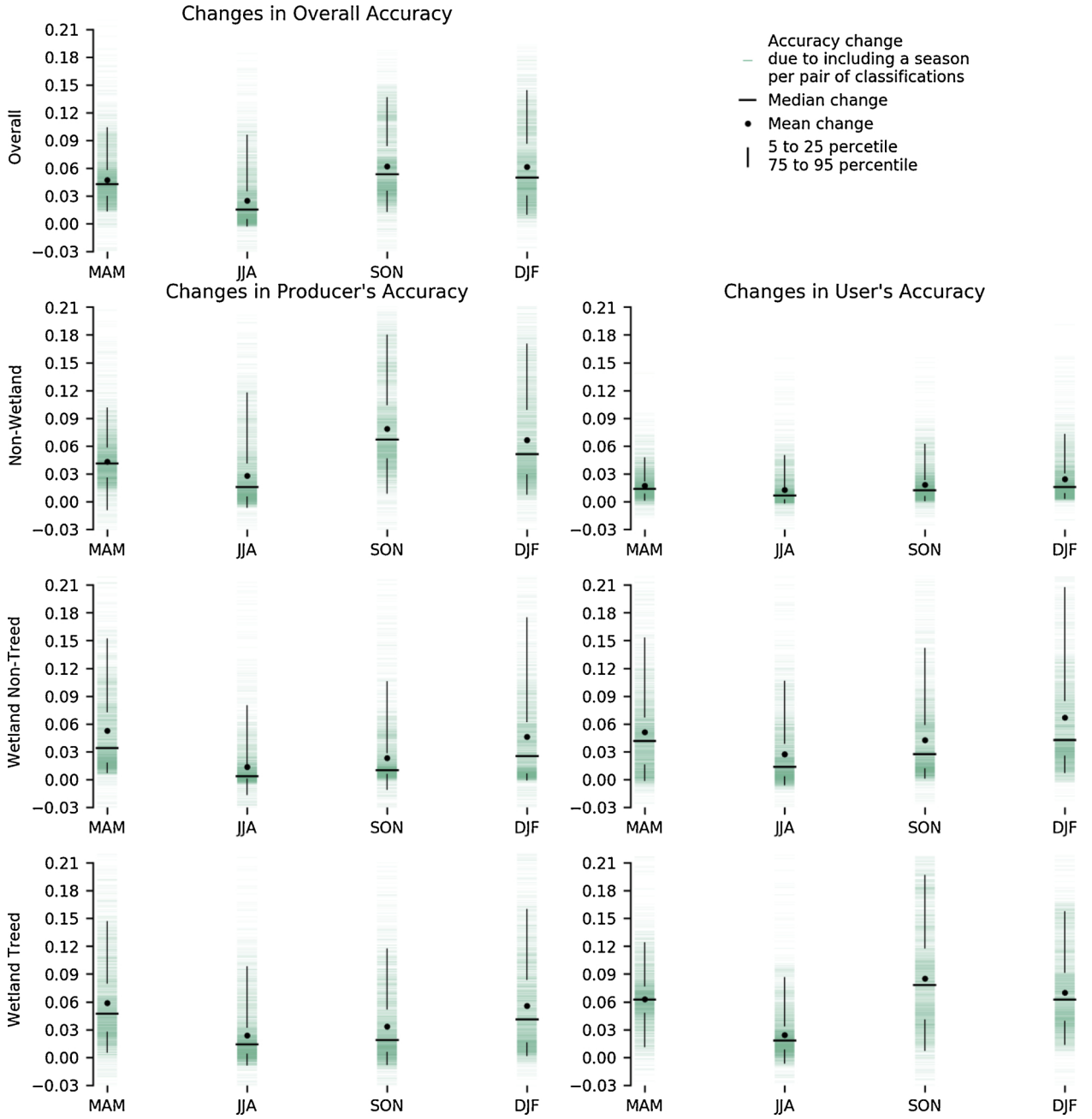

Fig. 7. Changes in classification accuracies between using and not using observations of each season.

MAM and DJF (Fig. 7) also indicates the usefulness of Sentinel-1 data acquired during the wetter and colder seasons of the year in this study area, especially with regard to the producer's and user's accuracies of treed and non-treed wetlands. Further studies are needed to investigate mechanisms in detail behind the usefulness of Sentinel-1 features from wet and cold seasons when the presence of snow and ice are most probable, such as the differences in C-band SAR responses to different interactions between snow/ice and different vegetation structures (trees versus non-trees).

Herein we demonstrated the utility of the within-year temporal information of the Sentinel-1 time series to differentiate treed and non-treed wetlands. The top-performing classifications used all available observations from the entire year, covering all the seasons. The direct use of available observations in the RF classifier resulted in higher accuracies than the generalized temporal forms considered (e.g. monthly or seasonal means), suggesting that these generalized forms lack the same level of information to accurately differentiate treed- and non-treed wetlands. Even when missing observations occur, the direct use of all available observations is still the top performing temporal form for the RF classifier after filling predictor values due to missing observations via a simple linear interpolation along the time axis (Fig. 8). This finding counters our intuition that the performance of classifications using an increasingly denser time series may be more negatively impacted by observation missing in various repeat observation cycles. The occurrence of missing observations can vary across space resulting in irregular observation dates and frequencies at the pixel-level, and can also vary across time resulting in different observation frequencies in different temporal periods of a year. Our random simulation of missing observations currently addresses the impact of the former case when different pixels across space have varying numbers of observations and possibly different dates of these observations. However, the current simulation does not address the latter case when missing observations

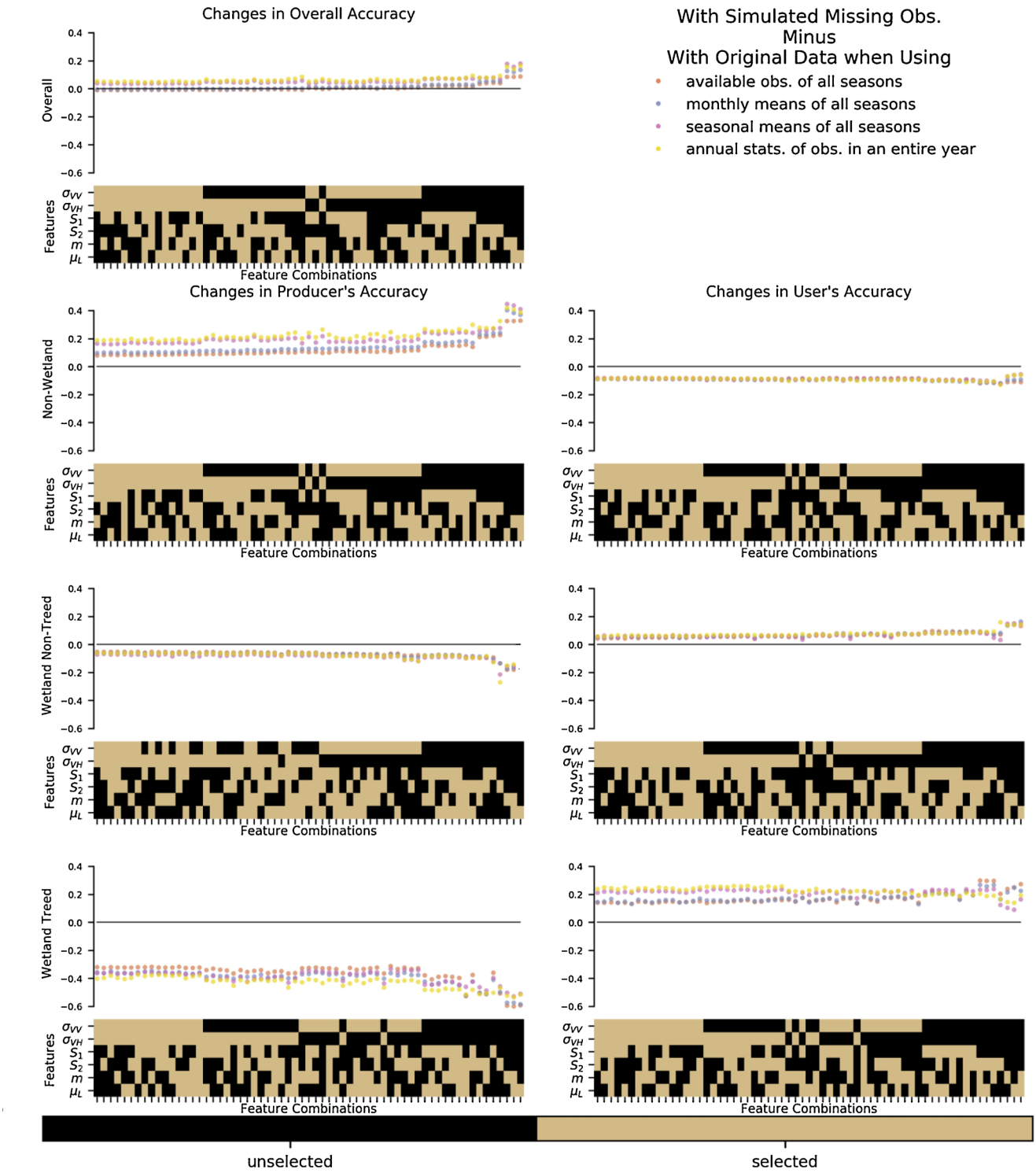

Fig. 8. Differences in classification accuracies between using synthetic data with simulated missing observations and using original data. The order of combinations in each panel are the same as Fig. 4.

occur differently in different time of a year because it assumes an equal missing probability of 0.24 in every repeat observation cycle. This assumption of the probability of missing observations is a simplification and other temporal patterns of missing data may result in different classification outcomes. For example, for the study area under investigation here, there were no Sentinel-1B observations in ESA's Copernicus Open Access Hub for the entire month of June. Such data gaps in the observation record could be due to satellite operation changes, such as orbital correction, software update, sensor recalibration, high priority tasking override, etcetera. If missing observations are temporally correlated or preferentially concentrated over some time of the year in Sentinel-1 time series, the question of whether the direct use of all available observations would continue to provide the best classification outcomes requires further investigations over larger area.

Furthermore, the temporal form seems to matter more than the feature combination for wetland classifications. The change in accuracies associated with different temporal forms in Fig. 6 is more pronounced than that associated with different feature combinations in

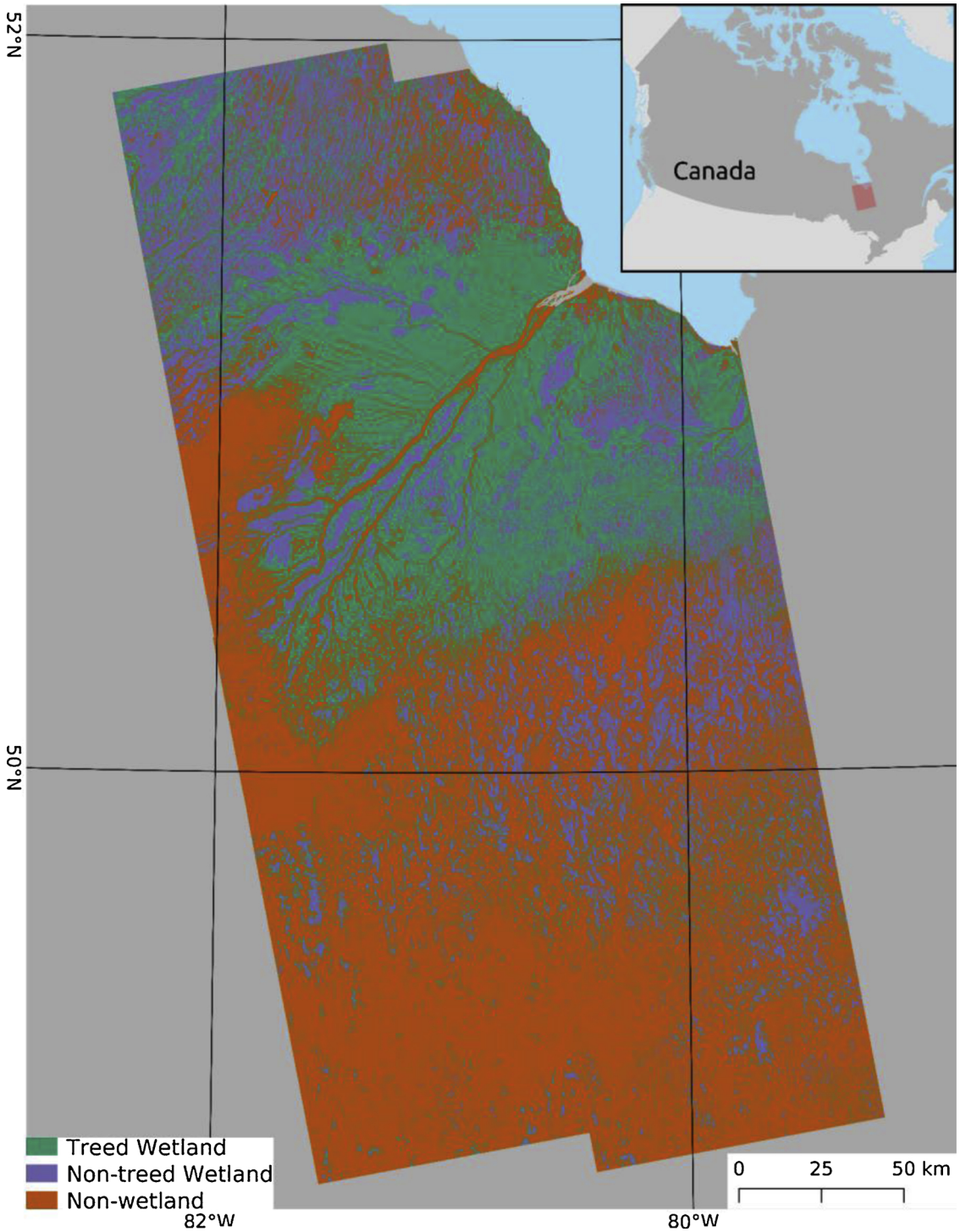

Fig. 9. Wetland classification using σ_{VH} and σ_{VV} from all available observations over the entire year of 2017.

Table 3
Error matrix of classification using σ_{VH} and σ_{VV} from all available observations over the entire year of 2017. Values are in terms of area proportions.

Map labels	Reference labels Non-wetland	Non-treed wetland	Treed wetland	User's accuracy
Non-wetland	0.473	0.003	0.021	0.952 ± 0.002
Non-treed wetland	0.023	0.199	0.005	0.877 ± 0.004
Treed wetland	0.085	0.003	0.188	0.683 ± 0.006
Producer's accuracy	0.814 ± 0.003	0.973 ± 0.002	0.879 ± 0.004	
Overall accuracy	**0.860 ± 0.002**			

Fig. 4. The spread of accuracy measures due to different feature combinations given a temporal form (Fig. 6) is also much narrower than the spread in accuracy measures that result from different temporal forms for a given a feature combination (Fig. 4). Such phenomena suggest the temporal information in the Sentinel-1 time series holds greater discriminant power over treed- and non-treed wetlands and non-wetlands than single observations of Sentinel-1 features. Therefore, while choosing optimal Sentinel-1 features for classification is important, choosing appropriate temporal forms of these features is at least equally, if not more, important for the classification of treed- and non-treed wetlands.

Although all the Sentinel-1 features carry some information for the classifications of treed- and non-treed wetlands (Fig. 3), the four features based on Stokes vector, S_1, S_2, m, and μ_L, resulted in only slight or no increases of accuracies when they are included into classifications (Fig. 5). These results support the use of σ_{VH} and σ_{VV} in large-scale processing of Sentinel-1 IW SLC data for the differentiation of treed and non-treed wetlands. As to the temporal forms of these two Sentinel-1 features, the results presented herein suggest the direct use of all available observations in an entire year provide the best classification outcomes. However, further investigations into classification performance when facing missing observations that are temporally correlated or preferentially concentrated in some period of the year are warranted. Nonetheless, a temporal form that uses Sentinel-1 observations from all the seasons of a year is recommended because it provides better performance for the objective stated herein of differentiating treed- and non-treed wetlands.

Our chosen best-performing classification (Fig. 9, Table 3) directly used σ_{VH} and σ_{VV} from all available observations over the entire year. In this classification, although the non-wetland class has the highest user's accuracy, it has the lowest producer's accuracy and the majority of omitted non-wetland pixels are mistaken as treed wetlands. Meanwhile, the treed wetland class has the lowest user's accuracy and its commission errors mainly result from the confusion between treed wetlands and non-wetlands. Non-treed wetlands are best identified among the three classes. The above findings about the accuracies corroborate the separability of wetland classes we observed from the value distributions of σ_{VV} and σ_{VH} over the three classes (Fig. 3), that is, treed wetlands and non-wetlands in our study area share similar values of σ_{VV} and σ_{VH} while non-treed wetlands have distinctive distributions of the feature values. In our study area, large parts of non-wetland areas are upland forests. The difference between upland forests and treed wetlands mainly lies in dry versus wet surfaces underneath vegetation cover (i.e. tree canopies and understory vegetation). Penetration of the C-band radar signal into vegetation cover is likely insufficient to aid in differentiating upland forests and treed wetlands in our study area. Moreover, upland forests and treed wetlands in this area may have similar within-year trajectories of canopy structure changes that were difficult for the Sentinel-1 data to differentiate. As a result, canopies of upland forests and treed wetlands induced similar time series of backscatter coefficients that did not notably improve the differentiation between the two in this area.

This study is intended to inform the characterization of wetlands, particularly the treed status of wetlands, over large areas such as the entire forest ecosystems of Canada. The current results demonstrated that time series of free and open Sentinel-1 IW products of operational global coverage are informative for the discrimination between treed and non-treed wetlands but may be limited for the discrimination between treed wetlands and non-wetlands, particularly upland forests. The separation between treed wetlands and non-wetlands over large areas may be improved by using additional remote sensing datasets of different types than C-band SAR, such as SAR data at longer wavelengths (e.g., L-band SAR data from Advanced Land Observing Satellite-2 (ALOS-2) (Kankaku et al., 2013) or from NASA-ISRO SAR mission (Rosen et al., 2015), and P-band SAR data from the BIOMASS mission (Quegan et al., 2019)) that can penetrate tree canopies with higher chances to reach underneath surfaces. Additionally, our current investigation does not address the effects of incidence angles on Sentinel-1 features as we only used the two nearest sub-swaths and the examination of the classification results showed no sign of artifacts caused by incidence angle. However, at national, continental or global scales, all the three sub-swaths of the Sentinel-1 acquisitions would have to be used altogether. The variation of incidence angles and its impact on wetland classifications need to be addressed explicitly to avoid any artifact. One solution could be to carry out classifications sub-swath by sub-swath to reduce the impacts of incidence angles. Another one could be to include local incidence angles as a predictor variable into classifiers and allow classifiers to treat pixels of different incidence angles differently, as demonstrated recently by Huang et al. (2018). The incidence direction of transmitted C-band waves to the ground also depends on whether observations are acquired during ascending or descending overpasses of the satellites. Our study area has only been covered by observations from ascending overpasses since 2016. When expanding the classification to larger areas where both ascending and descending observations are available, we anticipate value in investigating possible influences of differing incidence directions. Furthermore, as more years of Sentinel-1 data accumulate, it will become possible to investigate whether RF classifiers trained by observations from one year are transferrable to another year for wetland classification.

Furthermore, to systematically and routinely fulfill the potential of discriminating treed and non-treed wetlands over large areas, we need to expedite the critical preprocessing steps that are required to properly stack time series images for an appropriate utilization of temporal information in the Sentinel-1 data. Over the relatively small study area of this pilot study, the georegistration among Sentinel-1 images and also between the Sentinel-1 images and Landsat data was found of high fidelity through visual checking of suitable targets on the ground and a lack of artifacts emerging in the resultant classifications. Further, similarly accurate geospatial alignment between images from Sentinel-1 and other sensors onboard different satellites, such as Landsat, Sentinel-2, RADARSAT, ALOS-2, etc., can facilitate the synergetic use of multi-source Earth observation data including both passive optical and active radar, to further improve the characterization and monitoring of wetlands. Moreover, similar to cross-calibration efforts to ensure radiometric consistency of reflected signals in long-term optical observations to reduce artifacts in time series data (Chander et al., 2013; Markham and Helder, 2012; Roy et al., 2016), we need to maintain the radiometric consistency of backscatter signals through time to ensure the fidelity of temporal information for long-term studies and applications using Sentinel-1 data. All the aforementioned preprocessing efforts required for proper time series analysis have been recently encapsulated in the production of Analysis Ready Data for long term optical data, particularly data acquired by Landsat sensors (Dwyer et al., 2018; Wulder et al., 2019). Facilitating large-scale applications of Sentinel-1 time series data calls for similar efforts to produce ARD for the Sentinel-1 data archive as demonstrated recently by Truckenbrodt et al. (2019).

6. Conclusions

While SAR data deliver useful information on vegetation structure, soil moisture, and surface flooding, all of which are necessary for the study of wetlands, limited access to SAR datasets and complex preprocessing requirements have hampered the use of SAR observations to characterize wetlands over large areas and/or longtime periods. Free and open access to the Sentinel-1 SAR datasets, which have operational global coverage, provides improved temporal frequency of SAR data over greater spatial extents, thereby opening numerous opportunities to improve our understanding of wetlands. In this study, we found the greatest utility in the backscatter coefficients of VV and VH polarization (σ_{VV} and σ_{VH}) amongst the six examined Sentinel-1 features for the classification of treed and non-treed wetlands and non-wetlands. The

temporal information in the Sentinel-1 features is valuable to our wetland classification. Choosing an appropriate temporal form of Sentinel-1 features is equally, if not more important than choosing an appropriate combination of features. Using observations from all the seasons of the year often yielded higher accuracy than using fewer seasons. Moreover, directly using all within-year observations often yielded higher accuracy as a result of providing the classifier with richer and fuller temporal information on wetlands, compared to the use of more generalized temporal forms such as monthly/seasonal means or annualized statistics. By using σ_{VV} and σ_{VH} from all available observations in the year of 2017, we achieved an overall accuracy of 0.860 ± 0.002, with non-treed wetlands mapped with the highest accuracy and the majority of class confusion between treed wetlands and non-wetlands. Based on our simulation of missing observations that are equally probable in each repeat observation cycle, missing observations did not reduce the overall accuracy of the classifications that directly used all within-year observations. Insights gained from the results presented herein are useful for informing large-area utilization of Sentinel-1 time series for improved discrimination of treed and non-treed wetland classes.

Acknowledgements

This research was undertaken as part of the “Earth Observation to Inform Canada’s Climate Change Agenda (EO3C)” project jointly funded by the Canadian Space Agency (CSA), Government Related Initiatives Program (GRIP), and the Canadian Forest Service (CFS) of Natural Resources Canada (NRCan). This research was enabled in part by the computational support provided by WestGrid (www.westgrid.ca) and Compute Canada (www.computecanada.ca).

References

Abercrombie, S.P., Friedl, M.A., 2016. Improving the consistency of multitemporal land cover maps using a hidden Markov model. IEEE Trans. Geosci. Remote Sens. 54, 703–713. https://doi.org/10.1109/TGRS.2015.2463689.

Abraham, K.F., McKinnon, L.M., 2011. Hudson plains Ecozone+ evidence for key findings summary. Canadian Biodiversity: Ecosystem Status and Trends 2010, Evidence for Key Findings Summary Report No. 2. Ottawa, ON. URL. http://www.biodivcanada.ca/default.asp?lang=En&n=137E1147-1.

Adam, E., Mutanga, O., Rugege, D., 2010. Multispectral and hyperspectral remote sensing for identification and mapping of wetland vegetation: a review. Wetl. Ecol. Manag. 18, 281–296. https://doi.org/10.1007/s11273-009-9169-z.

Amani, M., Salehi, B., Mahdavi, S., Brisco, B., 2019. Separability analysis of wetlands in Canada using multi-source SAR data. GIScience Remote Sens. 1–28. https://doi.org/10.1080/15481603.2019.1643530.

Banks, S., White, L., Behnamian, A., Chen, Z., Montpetit, B., Brisco, B., Pasher, J., Duffe, J., 2019. Wetland classification with multi-angle/temporal SAR using random forests. Remote Sens. 11, 670. https://doi.org/10.3390/rs11060670.

Belgiu, M., Drăgu, L., 2016. Random forest in remote sensing: a review of applications and future directions. ISPRS J. Photogramm. Remote Sens. 114, 24–31. https://doi.org/10.1016/j.isprsjprs.2016.01.011.

Bourgeau-Chavez, L.L., Endres, S., Powell, R., Battaglia, M.J., Benscoter, B., Turetsky, M., Kasischke, E.S., Banda, E., 2016. Mapping boreal peatland ecosystem types from multitemporal radar and optical satellite imagery. Can. J. For. Res. 47, 545–559. https://doi.org/10.1139/cjfr-2016-0192.

Breiman, L., 2001. Random forests. Mach. Learn. 45, 5–32. https://doi.org/10.1023/A:1010933404324.

Brisco, B., Kapfer, M., Hirose, T., Tedford, B., Liu, J., 2011. Evaluation of C-band polarization diversity and polarimetry for wetland mapping. Can. J. Remote Sens. 37, 82–92. https://doi.org/10.5589/m11-017.

Brisco, B., Li, K., Tedford, B., Charbonneau, F., Yun, S., Murnaghan, K., 2013. Compact polarimetry assessment for rice and wetland mapping. Int. J. Remote Sens. 34, 1949–1964. https://doi.org/10.1080/01431161.2012.730156.

Canada’s National Forest Inventory, 2017. National Forest Inventory Photo Plot Data Dictionary For Second Remeasurement V6.0. Victoria, BC, Canada. URL. https://nfi.nfis.org/en/photo_plot.

Canada’s National Forest Inventory, 2010. Unpublished Analysis of Data by Ecozone+ From: Canada’s National Forest Inventory Standard Reports [WWW Document]. URL https://nfi.nfis.org/en/standardreports (Accessed 3.1.10). .

Chander, G., Mishra, N., Helder, D.L., Aaron, D.B., Angal, A., Choi, T., Xiong, X., Doelling, D.R., 2013. Applications of spectral band adjustment factors (SBAF) for cross-calibration. IEEE Trans. Geosci. Remote Sens. 51, 1267–1281. https://doi.org/10.1109/TGRS.2012.2228007.

Cloude, S.R., Goodenough, D.G., Chen, H., 2012. Compact decomposition theory. IEEE Geosci. Remote Sens. Lett. 9, 28–32. https://doi.org/10.1109/LGRS.2011.2158983.

Comber, A., Wulder, M.A., 2019. Considering spatiotemporal processes in big data analysis: insights from remote sensing of land cover and land use. Trans. GIS. https://doi.org/10.1111/tgis.12559. tgis.12559.

Corcoran, J.M., Knight, J.F., Gallant, A.L., 2013. Influence of multi-source and multi-temporal remotely sensed and ancillary data on the accuracy of random forest classification of wetlands in northern Minnesota. Remote Sens. 5, 3212–3238. https://doi.org/10.3390/rs5073212.

Dahl, T.E., Watmough, M.D., 2007. Current approaches to wetland status and trends monitoring in prairie Canada and the continental United States of America. Can. J. Remote Sens. 33, S17–S27. https://doi.org/10.5589/m07-050.

Davidson, N.C., Finlayson, C.M., 2007. Earth Observation for wetland inventory, assessment and monitoring. Aquat. Conserv. Mar. Freshw. Ecosyst. 17, 219–228. https://doi.org/10.1002/aqc.846.

Dwyer, J.L., Roy, D.P., Sauer, B., Jenkerson, C.B., Zhang, H.K., Lymburner, L., 2018. Analysis ready data: enabling analysis of the landsat archive. Remote Sens. 10, 1–19. https://doi.org/10.3390/rs10091363.

Ecological Stratification Working Group, 1995. A National Ecological Framework for Canada. Agriculture and Agri-Food Canada, Research Branch, Centre for Land and Biological Resources Research and Environment Canada, State of the Environment Directorate, Ecozone Analysis Branch, Ottawa/Hull.

Environment and Climate Change Canada, 2016. Canadian Environmental Sustainability Indicators: Extent of Canada’s Wetlands. URL. www.ec.gc.ca/indicateurs-indicators/default.asp?lang=en&n=69E2D25B-1.

ESA, 2019a. Interferometric Wide Swath [WWW Document]. Sentin. SAR User Guid. URL https://sentinel.esa.int/web/sentinel/user-guides/sentinel-1-sar/acquisition-modes/interferometric-wide-swath (Accessed 7.7.19). .

ESA, 2019b. Sentinel Application Platform (SNAP) [WWW Document]. URL https://step.esa.int/main/toolboxes/snap/ (Accessed 7.7.19). .

ESA, 2019c. Level-1 Interferometric Wide Swath SLC Products [WWW Document]. Sentin. SAR Tech. Guid. URL https://sentinel.esa.int/web/sentinel/technical-guides/sentinel-1-sar/products-algorithms/level-1/single-look-complex/interferometric-wide-swath (Accessed 7.7.19). .

European Union Copernicus, 2019. Copernicus Open Access Hub [WWW Document]. URL https://scihub.copernicus.eu/ (Accessed 6.14.19). .

FAO, 2012. Forest Resources Assessment Working Paper 180, FRA 2015, Terms and Definitions. FAO, Rome.

Finlayson, C.M., van der Valk, A.G., 1995. Wetland classification and inventory: a summary. Vegetatio 118, 185–192.

Fournier, R.A., Grenier, M., Lavoie, A., Hélie, R., 2007. Towards a strategy to implement the Canadian Wetland Inventory using satellite remote sensing. Can. J. Remote Sens. 33, S1–S16. https://doi.org/10.5589/m07-051.

Freeman, A., Durden, S.L., 1998. A three-component scattering model for polarimetric SAR data. IEEE Trans. Geosci. Remote Sens. 36, 963–973. https://doi.org/10.1109/36.673687.

Gallant, A., 2015. The challenges of remote monitoring of wetlands. Remote Sens. 7, 10938–10950. https://doi.org/10.3390/rs70810938.

Hansen, M.C., Potapov, P.V., Goetz, S.J., Turubanova, S., Tyukavina, A., Krylov, A., Kommareddy, A., Egorov, A., 2016. Mapping tree height distributions in Sub-Saharan Africa using Landsat 7 and 8 data. Remote Sens. Environ. https://doi.org/10.1016/j.rse.2016.02.023.

Hansen, M.C., Potapov, P.V., Moore, R., Hancher, M., Turubanova, S.A., Tyukavina, A., Thau, D., Stehman, S.V., Goetz, S.J., Loveland, T.R., Kommareddy, A., Egorov, A., Chini, L., Justice, C.O., Townshend, J.R.G., 2013. High-resolution global maps of 21st-Century forest cover change. Science (80-.) 342, 850–853.

Henderson, F.M., Lewis, A.J., 2008. Radar detection of wetland ecosystems: a review. Int. J. Remote Sens. 29, 5809–5835. https://doi.org/10.1080/01431160801958405.

Hermosilla, T., Wulder, M.A., White, J.C., Coops, N.C., Hobart, G.W., 2018. Disturbance-informed annual land cover classification maps of Canada’s forested ecosystems for a 29-Year landsat time series. Can. J. Remote Sens. 44, 1–21. https://doi.org/10.1080/07038992.2018.1437719.

Hermosilla, T., Wulder, M.A., White, J.C., Coops, N.C., Hobart, G.W., Campbell, L.B., 2016. Mass data processing of time series Landsat imagery: pixels to data products for forest monitoring. Int. J. Digit. Earth 9, 1035–1054. https://doi.org/10.1080/17538947.2016.1187673.

Huang, W., DeVries, B., Huang, C., Lang, M., Jones, J., Creed, I., Carroll, M., 2018. Automated extraction of surface water extent from Sentinel-1 data. Remote Sens. 10, 797. https://doi.org/10.3390/rs10050797.

Kankaku, Y., Suzuki, S., Osawa, Y., 2013. ALOS-2 mission and development status. 2013 IEEE International Geoscience and Remote Sensing Symposium - IGARSS 2396–2399. https://doi.org/10.1109/IGARSS.2013.6723302.

Klemas, V., 2013. Remote sensing of emergent and submerged wetlands: an overview. Int. J. Remote Sens. 34, 6286–6320. https://doi.org/10.1080/01431161.2013.800656.

Lang, M.W., McCarty, G.W., 2008. Remote sensing data for regional wetland mapping in the United States: trends and future prospects. In: Russo, R.E. (Ed.), Wetlands: Ecology, Conservation and Restoration. Nova Science Publishers, Inc., Hauppauge, New York, pp. 73–112.

Lee, J.-S., Lee, J.-S., Wen, J.-H., Ainsworth, T.L.L., Chen, K.-S., Chen, A.J.J., Lee, Jong-Sen, Lee, Jong-Sen, Wen, Jen-Hung, Ainsworth, T.L.L., Chen, Kun-Shan, Chen, A.J.J., Lee, J.-S., Lee, J.-S., Wen, J.-H., Ainsworth, T.L.L., Chen, K.-S., Chen, A.J.J., 2009. Improved sigma filter for speckle filtering of SAR imagery. IEEE Trans. Geosci. Remote Sens. 47, 202–213. https://doi.org/10.1109/TGRS.2008.2002881.

Lunetta, R.S., Balogh, M.E., 1999. Application of multi-temporal Landsat 5 TM imagery for wetland identification. Photogramm. Eng. Remote Sensing 65, 1303–1310.

Mahdavi, S., Salehi, B., Amani, M., Granger, J.E., Brisco, B., Huang, W., Hanson, A., 2017. Object-based classification of wetlands in Newfoundland and labrador using multi-

temporal PolSAR data. Can. J. Remote Sens. 43, 432–450. https://doi.org/10.1080/07038992.2017.1342206.
Markham, B.L., Helder, D.L., 2012. Forty-year calibrated record of earth-reflected radiance from Landsat: a review. Remote Sens. Environ. 122, 30–40. https://doi.org/10.1016/j.rse.2011.06.026.
Martinez, J.M., Le Toan, T., 2007. Mapping of flood dynamics and spatial distribution of vegetation in the Amazon floodplain using multitemporal SAR data. Remote Sens. Environ. 108, 209–223. https://doi.org/10.1016/j.rse.2006.11.012.
Matthews, E., Fung, I., 1987. Methane emission from natural wetlands: global distribution, area, and environmental characteristics of sources. Global Biogeochem. Cycles 1, 61–86. https://doi.org/10.1029/GB001i001p00061.
Millennium Ecosystem Assessment, 2005. Ecosystems and Human Well-being: Wetlands and Water Synthesis. World Resources Institute, Washington, D.C. https://doi.org/10.1007/BF02987493.
Mitsch, W.J., Gosselink, J.G., 2007. Wetlands, 4th ed. John Wiley Sons, Inc.
NASA JPL, 2019. SRTM C-band Data Products [WWW Document]. URL https://www2.jpl.nasa.gov/srtm/cbanddataproducts.html (Accessed 7.7.19). .
National Wetlands Working Group, 1997. The Canadian Wetland Classification System. URL. National Wetlands Working Group, Waterloo, ON, Canada. http://library.wur.nl/WebQuery/clc/1783071.
Pedregosa, F., Varoquaux, G., Gramfort, A., Michel, V., Thirion, B., Grisel, O., Blondel, M., Prettenhofer, P., Weiss, R., Dubourg, V., Vanderplas, J., Passos, A., Cournapeau, D., Brucher, M., Perrot, M., Duchesnay, É., 2011. Scikit-learn: machine learning in Python. J. Mach. Learn. Res. 12, 2825–2830.
Pekel, J.-F., Cottam, A., Gorelick, N., Belward, A.S., 2016. High-resolution mapping of global surface water and its long-term changes. Nature 540, 418–422. https://doi.org/10.1038/nature20584.
Quegan, S., Le Toan, T., Chave, J., Dall, J., Exbrayat, J., Minh, D.H.T., Lomas, M., D'Alessandro, M.M., Paillou, P., Papathanassiou, K., Rocca, F., Saatchi, S., Scipal, K., Shugart, H., Smallman, T.L., Soja, M.J., Tebaldini, S., Ulander, L., Villard, L., Williams, M., 2019. The european space agency BIOMASS mission: measuring forest above-ground biomass from space. Remote Sens. Environ. 227, 44–60. https://doi.org/10.1016/j.rse.2019.03.032.
Ramsar Convention Secretariat, 2013. The Ramsar Convention Manual: a Guide to the Convention on Wetlands (Ramsar, Iran, 1971), 6th ed. Ramsar Convention Secretariat, Gland, Switzerland. https://doi.org/10.1007/978-94-007-0551-7.
Raney, R.K., 2006. Dual-polarized SAR and stokes parameters. IEEE Geosci. Remote Sens. Lett. 3, 317–319. https://doi.org/10.1109/LGRS.2006.871746.
Rosen, P.A., Hensley, S., Shaffer, S., Veilleux, L., Chakraborty, M., Misra, T., Bhan, R., Sagi, V.R., Satish, R., 2015. The NASA-ISRO SAR mission - an international space partnership for science and societal benefit. 2015 IEEE Radar Conference (RadarCon) 1610–1613. https://doi.org/10.1109/RADAR.2015.7131255.
Roy, D.P., Kovalskyy, V., Zhang, H., Vermote, E.F., Yan, L., Kumar, S.S., Egorov, A., 2016. Characterization of Landsat-7 to Landsat-8 reflective wavelength and normalized difference vegetation index continuity. Remote Sens. Environ. https://doi.org/10.1016/j.rse.2015.12.024.
Thogmartin, W.E., Sauer, J.R., Knutson, M.G., 2004. A hierarchical spatial model of avian abundance with application to cerulean warblers. Ecol. Appl. 14, 1766–1779. https://doi.org/10.1890/03-5247.
Tiner, R.W., 2016. Wetland Indicators: a Guide to Wetland Formation, Identification, Delineation, Classification, and Mapping, 2nd ed. CRC press, Boca Raton, FL.
Tiner, R.W., Lang, M.W., Klemas, V.V., 2015. Remote Sensing of Wetlands: Applications and Advances, 1st ed. CRC press, Boca Raton, FL.
Toner, M., Keddy, P., 1997. River hydrology and riparian wetlands: a predictive model for ecological assembly. Ecol. Appl. 7, 236–246. https://doi.org/10.1890/1051-0761(1997)007[0236:RHARWA]2.0.CO;2.
Torres, R., Snoeij, P., Geudtner, D., Bibby, D., Davidson, M., Attema, E., Potin, P., Rommen, B., Floury, N., Brown, M., Traver, I.N., Deghaye, P., Duesmann, B., Rosich, B., Miranda, N., Bruno, C., L'Abbate, M., Croci, R., Pietropaolo, A., Huchler, M., Rostan, F., 2012. GMES Sentinel-1 mission. Remote Sens. Environ. 120, 9–24. https://doi.org/10.1016/j.rse.2011.05.028.
Töyrä, J., Pietroniro, A., Martz, L.W., 2001. Multisensor hydrologic assessment of a freshwater wetland. Remote Sens. Environ. 75, 162–173. https://doi.org/10.1016/S0034-4257(00)00164-4.
Truckenbrodt, J., Freemantle, T., Williams, C., Jones, T., Small, D., Dubois, C., Thiel, C., Rossi, C., Syriou, A., Giuliani, G., 2019. Towards Sentinel-1 SAR analysis-ready data: a best practices assessment on preparing backscatter data for the cube. Data 4, 93. https://doi.org/10.3390/data4030093.
Tsyganskaya, V., Martinis, S., Marzahn, P., Ludwig, R., 2018. SAR-based detection of flooded vegetation – a review of characteristics and approaches. Int. J. Remote Sens. 39, 2255–2293. https://doi.org/10.1080/01431161.2017.1420938.
White, L., Brisco, B., Dabboor, M., Schmitt, A., Pratt, A., 2015. A collection of SAR methodologies for monitoring wetlands. Remote Sens. 7, 7615–7645. https://doi.org/10.3390/rs70607615.
Wulder, M.A., Li, Z., Campbell, E., White, J.C., Hobart, G., Hermosilla, T., Coops, N.C., 2018. A national assessment of wetland status and trends for Canada's forested ecosystems using 33 years of earth observation satellite data. Remote Sens. 10, 1623. https://doi.org/10.3390/rs10101623.
Wulder, M.A., Loveland, T.R., Roy, D.P., Crawford, C.J., Masek, J.G., Woodcock, C.E., Allen, R.G., Anderson, M.C., Belward, A.S., Cohen, W.B., Dwyer, J., Erb, A., Gao, F., Griffiths, P., Helder, D., Hermosilla, T., Hipple, J.D., Hostert, P., Hughes, M.J., Huntington, J., Johnson, D.M., Kennedy, R., Kilic, A., Li, Z., Lymburner, L., McCorkel, J., Pahlevan, N., Scambos, T.A., Schaaf, C., Schott, J.R., Sheng, Y., Storey, J., Vermote, E., Vogelmann, J., White, J.C., Wynne, R.H., Zhu, Z., 2019. Current status of Landsat program, science, and applications. Remote Sens. Environ. 225, 127–147. https://doi.org/10.1016/j.rse.2019.02.015.
Wulder, M.A., White, J.C., Bater, C.W., Coops, N.C., Hopkinson, C., Chen, G., 2012. Lidar plots — a new large-area data collection option: context, concepts, and case study. Can. J. Remote Sens. 38, 600–618. https://doi.org/10.5589/m12-049.
Wulder, M.A., White, J.C., Cranny, M., Hall, R.J., Luther, J.E., Beaudoin, A., Goodenough, D.G., Dechka, J.A., 2008. Monitoring Canada's forests. Part 1: completion of the EOSD land cover project. Can. J. Remote Sens. 34, 549–562. https://doi.org/10.5589/m08-066.
Yamazaki, D., Trigg, M.A., Ikeshima, D., 2015. Development of a global ~90m water body map using multi-temporal Landsat images. Remote Sens. Environ. 171, 337–351. https://doi.org/10.1016/j.rse.2015.10.014.
Yommy, A.S., Liu, R., Wu, A.S., 2015. SAR image despeckling using refined Lee filter. 2015 7th International Conference on Intelligent Human-Machine Systems and Cybernetics 260–265. https://doi.org/10.1109/IHMSC.2015.236.
Zhang, X., Treitz, P.M., Chen, D., Quan, C., Shi, L., Li, X., 2017. Mapping mangrove forests using multi-tidal remotely-sensed data and a decision-tree-based procedure. Int. J. Appl. Earth Obs. Geoinf. 62, 201–214. https://doi.org/10.1016/j.jag.2017.06.010.
Zhao, L., Yang, J., Li, P., Zhang, L., 2014. Seasonal inundation monitoring and vegetation pattern mapping of the Erguna floodplain by means of a RADARSAT-2 fully polarimetric time series. Remote Sens. Environ. 152, 426–440. https://doi.org/10.1016/j.rse.2014.06.026.